JAERI-M
6934

THE EFFECTS OF THE CAPTURE GAMMA-RAY SPECTRA ON THE ABSORBED DOSE

——ANALYTICAL STUDY——

February 1977

Nobuo SASAMOTO and Shun-ichi TANAKA

日本原子力研究所
Japan Atomic Energy Research Institute

JAERI-M 6934

The Effects of the Capture Gamma-ray Spectra on the Absorbed Dose - Analytical Study

Nobuo SASAMOTO and Shun-ichi TANAKA

Division of Reactor Engineering, Tokai,
JAERI

(Received January 26, 1977)

The effect upon the absorbed dose of the differences in capture gamma-ray yields due to thermal neutron capture has been examined using the yield data of aluminum and iron in POPOP4 library. The absorbed doses normalized to energy deposition of the emitted capture gamma rays agree well within accuracy of absorbed dose measurements. Important criteria for selecting the capture gamma-ray yield data are the total energy release and the average energy of the emitted capture gamma rays.

JAERI－M 6934

捕獲ガンマ線スペクトルの吸収線量への影響
－解析的研究－

日本原子力研究所東海研究所原子炉工学部
笹本　宣雄・田中　俊一

（1977年1月26日受理）

熱中性子捕獲ガンマ線スペクトルの違いが体系内の吸収線量におよぼす影響を，鉄とアルミニウムについて解析的に検討した。解析の結果，仮想的な捕獲ガンマ線エネルギー吸収量で規格化した体系内の吸収線量は，捕獲ガンマ線スペクトルに関係なく実験精度の範囲内で一致した。したがって捕獲ガンマ線データの選択基準としては，捕獲ガンマ線の全放出エネルギーと平均エネルギーを考えれば良いことがわかった。

CONTENTS

1. Introduction

Neutron capture reaction consists of the absorption of neutrons by the nucleus and the emission of one or more gamma rays. The capture gamma rays due to the neutron capture reaction are often the dominant sources in radiation heating and in shielding of fission reactor.

Capture gamma-ray yields resulting from the capture of thermal neutrons have been measured for most of the elements. On the other hand, however, only few yield data have been measured for nonthermal neutron capture reactions. Measurement of capture gamma-ray yield is being made increasing in nonthermal regions, and Yost et al.[1,2] have theoretically investigated the capture gamma-ray yield as a function of the incident neutron energy. However, one is forced to use the assumption on the shielding calculation that the capture gamma-ray yield from the capture of nonthermal neutrons is the same as that from thermal neutrons, because of the lack of evaluated nonthermal data. A number of measured capture gamma-ray yields in thermal neutron captures are summarized in the POPOP4 library[3] and others.[4,5] However among these data, there are large differences in spectrum shape and emission probability of the capture gamma rays.

Subjects in shielding calculation concerning capture gamma rays are thus (1) the accumulation of measured yield data due to nonthermal neutron captures, and (2) evaluation of the gamma rays due to thermal neutron captures.

One of the important objects in shielding calcualtion is to estimate the absorbed dose in reactor materials. At present, shielding calculations are made by solving the neutron and

gamma-ray coupled transport problem using the multigroup constants which are produced by coupling the neutron group constants and the gamma-ray group constants. In this paper, the effect upon the absorbed dose of the differences among the capture gamma-ray yield was investigated analytically by using one dimensional discrete ordinate transport code ANISN.[6] That is, the space-dependent absorbed doses in homogeneous aluminum and iron of spherical geometries were calculated using the various capture gamma-ray yield data, and the differences among the doses calculated were investigated in connection with properties of the capture gamma-ray yields.

2. POPOP4 Library

The POPOP4 library is compiled at RSIC (Radiation Shielding Information Center) of ORNL. The library includes secondary gamma-ray yields and secondary gamma-ray production cross sections :

(n:γ) radiative capture, (n:α,γ), (n:2n',γ), (n:3n',γ), (n:p,γ), (n:other charged particles,γ) and (n:γ) fission reaction.

In the library, 244 secondary gamma-ray data sets for 79 nuclides are compiled. The capture gamma-ray data account for nearlly 80 % of the library, and besides most of the data are for thermal neutron captures. Respective capture gamma-ray yields are given in one of the following three formats :

1) discrete spectrum (characteristic energy)
2) spectrum in histogram
3) discrete spectrum (representative energy)

Usually two or more data sets are contained in each neutron capture reaction of a nucleus : no evaluation nor recommendation is made of the data sets.

3. Calculational Model of Absorbed Dose

The space-dependent neutron and gamma-ray spectra and the absorbed doses were calculated by using one-dimensional anisotropic discrete ordinate transport code ANISN. The absorbed dose D_{ab} is calculated using the gamma-ray flux spectrum by the following :

$$D_{ab} = \sum_{I} (\phi_{\gamma}^{I} \cdot {}_{m}\mu_{en}^{I} \cdot E^{I}) \quad , \tag{1}$$

where ϕ_{γ}^{I} : gamma-ray flux in I-th group

${}_{m}\mu_{en}$: mass energy absorption coefficient of I-th group referred to E. Storm et al.[7)]

E^{I} : average gamma-ray energy of I-th group

The tabulated ${}_{m}\mu_{en}$ data of aluminum and iron used in the calculations are shown in Table I, and the curves of ${}_{m}\mu_{en}$ and of the products of ${}_{m}\mu_{en}$ and E^{I} are presented in Fig.1.

The gamma-ray spectra and absorbed doses were calcualted by P_3- S_{16} approximation under the calculational conditions as follows :

1) source : point isotropic neutron source having the fission spectrum. Sources are distributed only at the first mesh interval with mesh width 0.5 cm for aluminum and 0.25 cm for iron

2) geometry : aluminum sphere with radius 100 cm and iron sphere with radius 25 cm.

3) mesh width :

for aluminum, 0.25 cm for the first two intervals and 0.50 cm for the rest

for iron , 0.50 cm for the first two intervals and 1.00 cm for the rest

4) energy group : 26 groups for neutrons covering the energy range from 14 MeV to 0.001 eV, and 20 groups for gamma rays from 10 MeV to 0.1 MeV. The energy group structure is shown in Table II for neutrons, and that for gamma rays is already presented in Table I together with the $_{m}\mu_{en}$ values.

The neutron and gamma-ray coupled multigroup constants used in the calculation were produced from the ENDF/B-IV libraries and the POPOP4 library using the revised group constant production code system RADHEAT V-3[8] which was modified so that the self-shielding factors can be taken into account on the cross sections of resonance region.

Under the above calculational conditions, it is expected that the effect of the differences among the capture gamma-ray yields upon the absorbed dose is clarified from the calculated results by ANISN code without ambiguity of the calcualtional method and geometrical conditions. In the present study, three kinds of capture gamma-ray yield data due to thermal neutron capture contained in the POPOP4 library are investigated for aluminum and iron. These data are indicated below by the same identification numbers as those in the POPOP4 library.

aluminum : 130102, 130103, 130104

iron : 260101, 260103, 260108

The groupwise capture gamma-ray yield data are shown in Figs. 2 and 3.

4. Calculational Results

The calculated gamma-ray spectra at 60 cm and 15 cm from the center of aluminum and iron spheres respectively are shown in Figs.4 and 5. It is seen that there are remarkable differences among the gamma-ray spectra calculated using various capture gamma-ray yield data. In Fig.6 is shown the absorbed dose distribution in the aluminum sphere obtained from eq.(1) by gamma-ray spectrum calculation. The absorbed dose distribution in the iron sphere is shown in Fig.7. In both the aluminum and the iron sphere, the tendency is similar that the absorbed dose varies monotonously as a function of the distance from the sphere center (source location), but the differences are large especially in the aluminum. For instance, the absorbed doses by data set 130102 are nearlly twice as large as those by data set 130104.

Then we will introduce the normalized absorbed dose D^*_{ab} as follows.

$$D^*_{ab} = \frac{\sum_I (\phi^I_\gamma \cdot m\mu_{en}(E^I) \cdot E^I)}{m\mu_{en}(\bar{E}) \cdot \sum_i E_i Y_i} \quad , \tag{2}$$

where Y_i is the yield of gamma rays having energy E_i emitted by one thermal neutron absorption and $\bar{E}$ is the average energy defined as

$$\bar{E} = \frac{\sum_i (E_i Y_i \cdot m\mu_{en}(E_i))}{\sum_i (Y_i \cdot m\mu_{en}(E_i))} \quad . \tag{3}$$

Hereafter, the denominator in eq.(2) is denoted as the normalization factor.

In Fig.8 are shown the ratios of the normalized absorbed doses in the aluminum sphere by data sets 130102 and 130103 to that by data set 130104. Here, the ratio R_j of the absorbed dose by data set j to that by data set k is expressed as

$$R_j = \frac{(\sum_I \phi^I_\gamma \cdot {}_m\mu_{en}(E^I)\cdot E^I)_j}{(_m\mu_{en}(\bar{E})\sum_i E_i Y_i)_j} \Big/ \frac{(\sum_I \phi^I \cdot {}_m\mu_{en}(E^I)\cdot E^I)_k}{(_m\mu_{en}(\bar{E})\sum_i E_i Y_i)_k} \quad . \tag{4}$$

Also, the ratios of the normalized absorbed doses in the iron sphere by data sets 260103 and 260108 to that by data set 260101 are shown in Fig.9. As is evident from Fig.8, the normalized ratios in aluminum exhibit the space dependency particularly in the vicinity of the neutron source and also of the outer boundary to vacuum space. On the other hand, also the normalized ratios in iron exhibit space dependency in the vicinity of the source, but they are presumably constant in the rest region. These space dependencies are not caused by the differences among the capture gamma-ray yields, but by the large gradient of neutron spectrum obtained by S_N transport calculation. Therefore, in order to examine the effect of the capture gamma-ray yield itself, it is necessary to see the ratios of the absorbed doses in the region where they hardly show space dependency. Then, we will examine only the ratios of doses at r=60 cm in the aluminum sphere and those at r=15 cm in the iron sphere. As seen in Fig.8 and 9, the normalized doses calculated using various capture gamma-ray yield data agree well within about 10 %. This deviation is considered to be within the accuracy of the absorbed dose measurement. But the unnormalized absorbed doses differ largely from one another.

In Table III are shown the ratios of both the unnormalized and normalized absorbed doses at the spacial points of interest, together with average energies $\bar{E}$ of the capture gamma-ray yield and the corresponding normalization factors.

5. Discussion and Conclusion

In the previous section, it has been shown that the absorbed doses normalized by the normalization factor of each capture gamma-ray yield data agree well.

Let us examine closely characteristics of the normalization factor. This factor means physically the energy deposition of the capture gamma rays in the material of interest. The mass energy absorption coefficient $_{m}\mu_{en}(E)$ for aluminum and iron depend on the gamma-ray energy, but there are not much functional changes in the energy region above 1.0 MeV. Actually, the average energies $\bar{E}$'s of the capture gamma-ray yield for aluminum take the values from 1.7 MeV for 130102 to 3.9 MeV for 130103, but the deviation among $_{m}\mu_{en}(E)$ is within 30 %. For iron data, the average energies take the values from 2.3 MeV for 260108 to 5.4 MeV for 260103 and their deviations of $_{m}\mu_{en}(E)$ are within only 7 %. Another component $\sum_{i}(E_i Y_i)$ means the total energy released per thermal neutron capture and it must be equivalent to the neutron binding energy of the target nucleus. However, the deviations of $\sum_{i}(E_i Y_i)$ among the data sets are about 60 % for aluminum and 6 % for iron.

Now, let us consider two kinds of capture gamma-ray yield data [A] and [B], and denote the absorbed doses calculated using these data as D_A and D_B respectively. The good agreement between the normalized absorbed doses suggests the relationship :

$$\frac{D_A}{{}_{m}\mu_{en}(\bar{E})_A \cdot \sum_{i}(E_i Y_i)_A} \cong \frac{D_B}{{}_{m}\mu_{en}(\bar{E})_B \cdot \sum_{i}(E_i Y_i)_B} , \qquad (5)$$

Eq.(5) is rewritten as

$$\frac{D_A}{D_B} \cong \frac{m^{\mu}en(\bar{E})_A \cdot \sum_i (E_i Y_i)_A}{m^{\mu}en(\bar{E})_B \cdot \sum_i (E_i Y_i)_B} , \qquad (6)$$

Following the result of the kinematics of the radiative-capture reaction, the values of $\sum_i (E_i Y_i)_A$ and $\sum_i (E_i Y_i)_B$ must be equivalent to the neutron binding energy E^{BE} of the target nucleus, regardless of the capture gamma-ray spectrum shape. Eq.(6) is rewritten using the binding energy E^{BE},

$$\frac{D_A}{D_B} \cong \frac{m^{\mu}en(\bar{E})_A \cdot E^{BE}}{m^{\mu}en(\bar{E})_B \cdot E^{BE}} .$$

$$= \frac{m^{\mu}en(\bar{E})_A}{m^{\mu}en(\bar{E})_B} \qquad (7)$$

The above results are summarized as follows.

1) The difference in calculated absorbed dose due to the different capture gamma-ray yields can be approximately predicted using the mass energy absorption coefficient corresponding to the average energy of each yield data.
2) If the total released energy is normalized to the binding energy, the effect upon the absorbed dose of the differences among the various capture gamma-ray yields is negligible, except for the region around the neutron source and the outer boundary, where the influence of the neutron and gamma-ray transport calcualtion on the absorbed dose exceeds that of the capture gamma-ray yield.
3) Important criteria for selecting the capture gamma-ray yield data are the total energy of the emitted capture gamma rays and the average energy.

The above conclusions derived for aluminum and iron will also apply to other elements or nuclides as long as the capture gamma-ray yield data for thermal neutron capture are concerned. However, it must be studied in the future whether or not the data for thermal neutron capture can be substituted by those for nonthermal neutron capture. In addition, it is necessary to compare the calculated absorbed dose with the experimental one for obtaining a final evaluation of the capture gamma-ray yield data.

For convenience in usage of capture gamma-ray yield data in the POPOP4 library, the index data for selection are listed in Appendix of the elements or nuclides important for shielding calculation. The index data include 1) name of element or nuclide, 2) neutron binding energy (E^{BE}),[9,10] 3) identification (ID), 4) total capture gamma rays ($\sum_i Y_i$), 5) total energy release ($\sum_i E_i Y_i$), and 6) $(\sum_i E_i Y_i)/E^{BE}$.

ACKNOWLEDGEMENTS

The authors would like to express their thanks to Y. Furuta for his valuable discussion in the course of this study. Thanks are also due to S. Miyasaka and K. Koyama for the use of the code system RADHEAT V-3.

REFERENCES

1) K. J. Yost, "A Method for the Calculation of Neutron Capture Gamma-ray Spectra," Nucl. Sci. Eng., 32, 62(1968).

2) J. E. White, C. Y. Fu and K. J. Yost, "Neutron Capture Gamma-ray Yields in Iron," Nucl. Sci. Eng., 51, 496(1973).

3) W. E. Ford, III, "The POPOP4 Library of Neutron-Induced Secondary Gamma-ray Yield and Cross Section Data," CTC-42, Oak Ridge Computer Technology Center(1970).

4) G. A. Bartholomew and L. A. Higgs, Compilation of Thermal Neutron Capture Gamma Rays, Canadian Report CRGP-784, Atomic Energy of Canada, Ltd., Chalk River Project, July 1958.

5) L. V. Groshev et al., Atlas of the Spectra of Gamma Rays from the Radiative Capture of Thermal Neutrons, Pergamon Press, Inc., New York, 1959.

6) W. W. Engle, Jr., "A USERS MANUAL FOR ANISN A One Dimensional Discrete Ordinates Transport Code With Anisotropic Scattering," K-1693(1967).

7) E. Storm and H. I. Israel, "Photon Cross Sections from 0.001 to 100 MeV for Elements 1 through 100, LA-3753(1967).

8) K. Koyama et al., to be published in JAERI-M report.

9) V. J. Ashly and H. C. Catron, Tables of Nuclear Reaction Q Values, UCRL-5419. Lawrence Radiation Laboratory, University of California, Livermore, Feb. 10, 1959.

10) W. E. Ford III, "Comparison of (n_{th},γ) Yields from the Current ENDF/B-III Data with Published Data," ORNL-TM-3910, Aug., 1972.

Table I

Gamma-ray Group Structure and Mass-Energy Absorption Coefficient

Grp. No.	Energy Range (MeV)		$\bar{E}$ (MeV)	$_{m}\mu_{en}$ (cm^2/gr)	
				Aluminum	Iron
1	10.0	9.0	9.5	0.0167	0.0213
2	9.0	8.0	8.5	0.0167	0.0209
3	8.0	7.0	7.5	0.0170	0.0206
4	7.0	6.0	6.5	0.0172	0.0203
5	6.0	5.0	5.5	0.0176	0.0200
6	5.0	4.0	4.5	0.0183	0.0198
7	4.0	3.0	3.5	0.0193	0.0199
8	3.0	2.0	2.5	0.0211	0.0209
9	2.0	1.0	1.5	0.0242	0.0238
10	1.0	0.9	0.95	0.0267	0.0262
11	0.9	0.8	0.85	0.0273	0.0267
12	0.8	0.7	0.75	0.0277	0.0273
13	0.7	0.6	0.65	0.0280	0.0281
14	0.6	0.5	0.55	0.0286	0.0288
15	0.5	0.4	0.45	0.0290	0.0298
16	0.4	0.3	0.35	0.0290	0.0318
17	0.3	0.25	0.275	0.0287	0.0356
18	0.25	0.20	0.225	0.0280	0.0420
19	0.20	0.15	0.175	0.0272	0.0582
20	0.15	0.10	0.125	0.0298	0.1210

Table II

Neutron Group Structure

Grp. No.	Energy Range (eV)		Grp. No.	Energy Range (eV)	
1	1.00×10^{7}	1.05×10^{7}	14	4.65×10^{3}	2.15×10^{3}
2	1.05×10^{7}	6.50×10^{6}	15	2.15×10^{3}	1.00×10^{3}
3	6.50×10^{6}	4.00×10^{6}	16	1.00×10^{3}	4.65×10^{3}
4	4.00×10^{6}	2.50×10^{6}	17	4.65×10^{3}	2.15×10^{3}
5	2.50×10^{6}	1.40×10^{6}	18	2.15×10^{3}	1.00×10^{3}
6	1.40×10^{6}	8.00×10^{5}	19	1.00×10^{3}	4.65×10^{2}
7	8.00×10^{5}	4.00×10^{5}	20	4.65×10^{2}	2.15×10^{2}
8	4.00×10^{5}	2.00×10^{5}	21	2.15×10^{2}	1.00×10^{2}
9	2.00×10^{5}	1.00×10^{5}	22	1.00×10^{2}	4.65×10^{1}
10	1.00×10^{5}	4.65×10^{4}	23	4.65×10^{1}	2.15×10^{1}
11	4.65×10^{4}	2.15×10^{4}	24	2.15×10^{1}	1.00×10^{1}
12	2.15×10^{4}	1.00×10^{4}	25	1.00×10^{-1}	4.65×10^{-1}
13	1.00×10^{4}	4.65×10^{3}	26	4.65×10^{-1}	1.00×10^{-3}

Table III

The ratios of the unnormalized and normalized absorbed doses, and the corresponding normalization factors.

ID No.	$\bar{E}$ (MeV)	(NF)†	Ratio	
			D_{ab}	D^{*}_{ab}
130102	1.68	0.277	1.865	0.943
130103	3.07	0.182	1.233	0.949
130104	3.94	0.140	1.000	1.000
260101	2.96	0.144	1.000	1.000
260103	5.37	0.149	1.036	1.002
260108	2.27	0.158	1.094	0.997

†) normalization factor : $_{m}\mu_{en}(\bar{E})\sum_{i}E_{i}Y_{i}$, $(MeV\cdot cm^{2}/gr)$

Appendix

Number of Photons and Total Energy Release Following Thermal Neutron Absorption

Element	E^{BE} (MeV)	ID No.	ΣY_i	$\Sigma E_i Y_i$ (MeV)	$(\Sigma E_i Y_i)/E^{BE}$
H	2.230	10101	1.00	2.230	1.000
Li		30101	2.59	8.904	
		30102	1.00	7.200	
Be	6.814	40101	2.07	9.097	1.335
		40102	1.25	6.803	0.998
		40103	1.27	6.540	0.960
B	11.451	50102	1.45	6.640	0.580
		50103	1.97	11.029	0.963
C	4.984	60101	1.25	4.899	0.983
		60102	1.30	4.950	0.993
		60103	1.00	4.000	0.803
N	10.806	70101	0.096	0.475	0.044
		70102	2.16	10.862	1.005
N^{14}	10.806	74103	1.87	10.920	1.008
Na	6.956	110101	1.88	6.240	0.897
		110102	1.88	6.233	0.896
		110103	5.11	11.720	1.685
Na^{23}	6.956	113101	3.57	6.873	0.988
		113102	4.46	11.228	1.614
Al	7.723	130101	1.75	7.393	0.957
		130102	6.40	11.787	1.526
		130103	2.65	9.180	1.189
		130104	1.77	7.450	0.965
		130105	1.68	7.279	0.942
		130106	2.77	9.200	1.191
		130107	6.00	10.970	1.420
Al^{27}	7.723	137101	2.11	6.053	0.784
		137102	2.12	7.099	0.919
Si	8.514	140101	2.26	9.288	1.091
		140102	2.63	10.501	1.233
		140103	2.28	9.305	1.093
		140104	2.17	9.041	1.062

		140105	2.34	9.575	1.125
		140106	2.97	6.753	0.793
Cl	7.970	170101	2.20	7.855	0.986
		170102	2.52	9.510	1.193
		170103	2.46	9.335	1.173
		170104	3.01	9.645	1.210
K	7.777	190101	2.07	5.843	0.751
		190102	2.32	7.526	0.968
		190103	2.32	7.472	0.961
		190104	3.86	9.976	1.283
Ca	8.336	200101	5.28	11.798	1.415
		200102	2.58	8.216	0.986
		200103	2.61	8.475	1.017
		200104	4.33	12.244	1.469
Cr	8.121	240101	0.90	0.432	0.053
		240102	2.27	5.879	0.724
		240103	2.27	7.185	0.885
		240104	1.87	9.227	1.136
Mn	7.267	250101	3.77	8.890	1.223
Mn^{55}	7.267	255101	2.50	5.358	0.737
Fe	7.777	260101	1.94	7.040	0.905
		260102	1.35	7.459	0.959
		260103	1.35	7.452	0.958
		260104	2.50	7.393	0.951
		260105	1.35	7.394	0.951
		260106	1.35	7.480	0.962
		260108	2.50	7.260	0.933
SUS		269101	1.41	7.785	
		269102	1.41	7.793	
Ni	8.590	280101	1.19	6.253	0.728
		280103	1.12	7.773	0.905
		280104	1.12	7.830	0.912
		280105	2.67	9.595	1.117
		280106	1.44	8.497	0.989
Cu	7.649	290103	1.59	7.910	1.034
		290104	1.60	7.931	1.037
		290105	1.53	7.849	1.026
		290106	1.59	7.911	1.034
		290107	2.07	7.198	0.941

		290108	2.41	7.955	1.040
Zr	7.088	400101	1.84	4.133	0.583
		400102	1.52	6.940	0.979
Nb	7.199	410101	0.68	3.032	0.421
		410102	2.86	7.239	1.006
		410103	2.86	7.239	1.006
Nb^{94}	8.452	414101	1.30	1.745	0.206
Mo		420101	1.57	2.787	
		420102	2.68	6.118	
		420103	3.58	8.783	
Cd	7.062	480101	1.85	2.821	0.399
		480102	4.14	8.485	1.202
Pb		820102	1.00	7.325	
		820104	1.00	7.860	
Pb^{204}		824101	1.71	6.805	
U^{238}		928102	0.85	1.341	
Pu		940102	6.11	19.925	

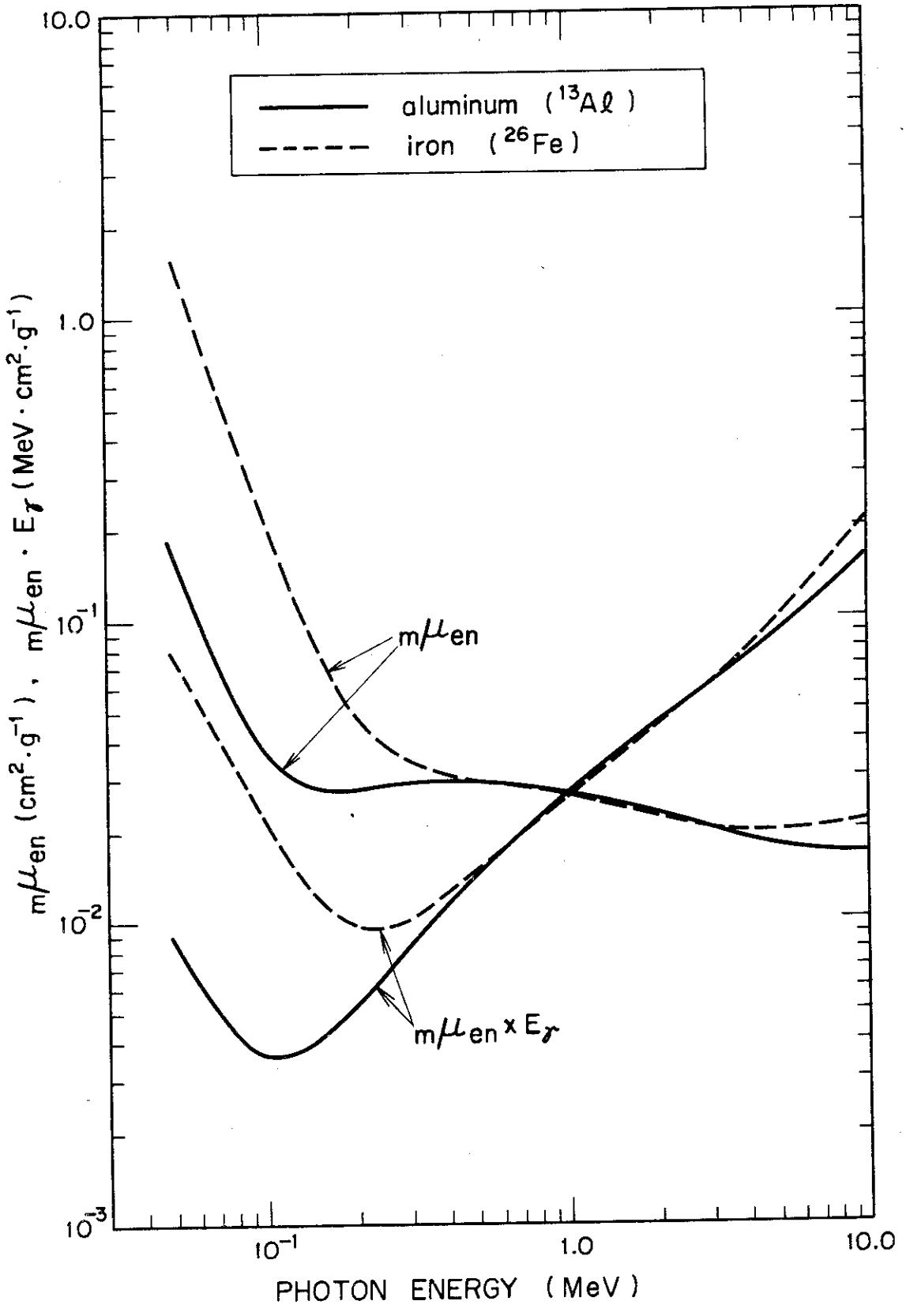

Fig. 1 Mass energy absorption coefficient $_{m}\mu_{en}$ and the product of $_{m}\mu_{en}$ and E^{I}.

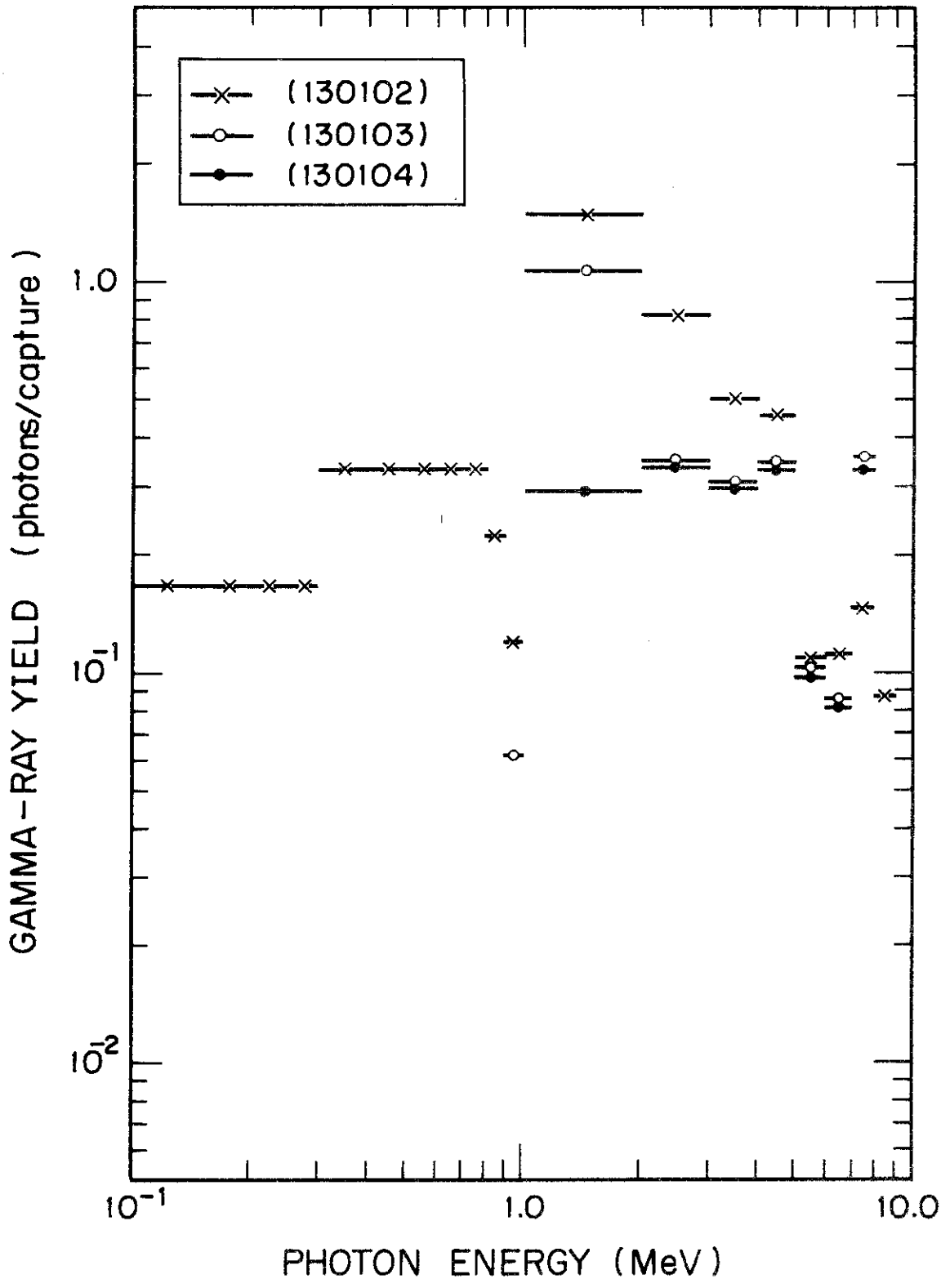

Fig. 2 Capture gamma-ray yield of aluminum.

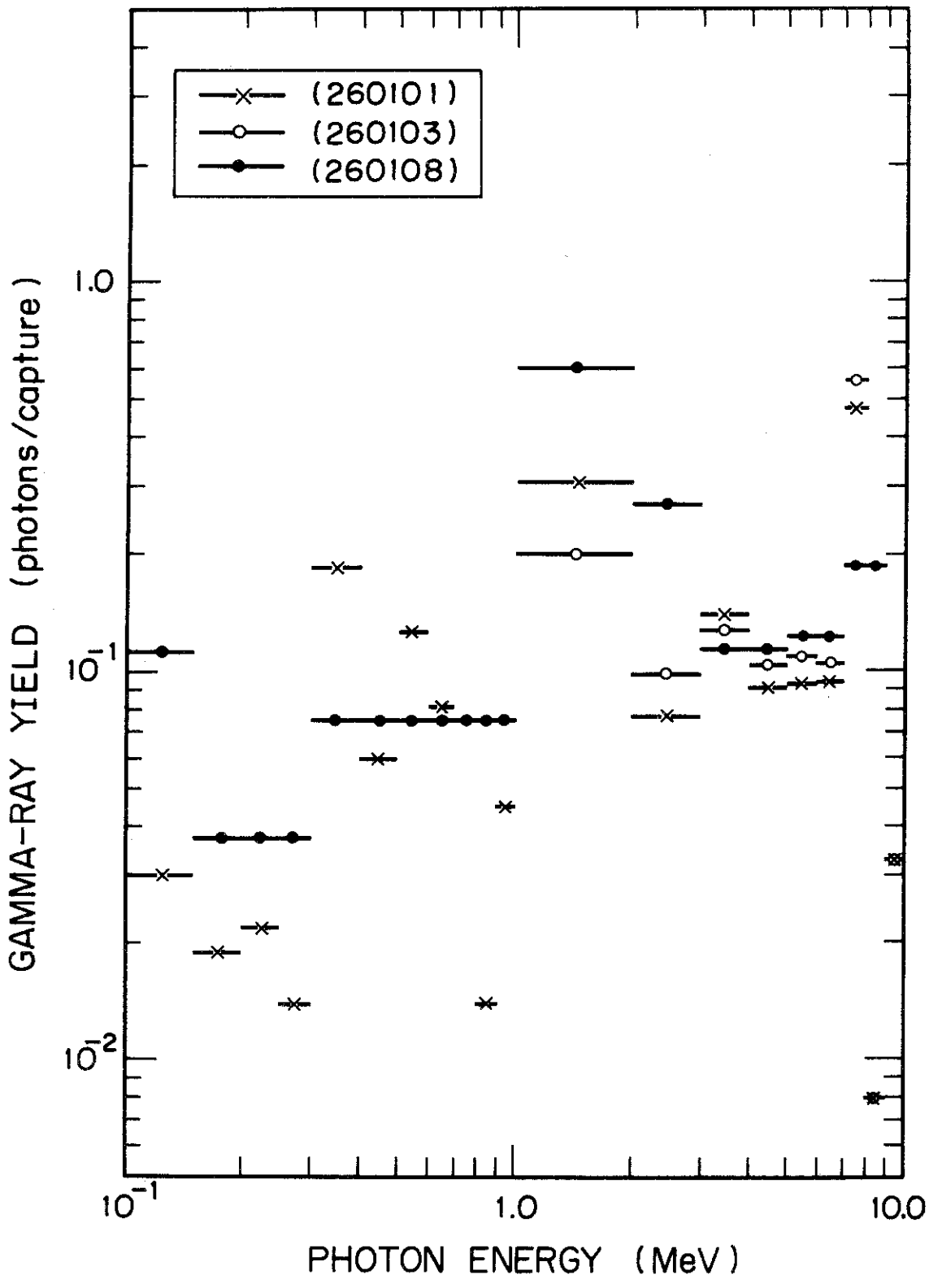

Fig. 3 Capture gamma-ray yield of iron.

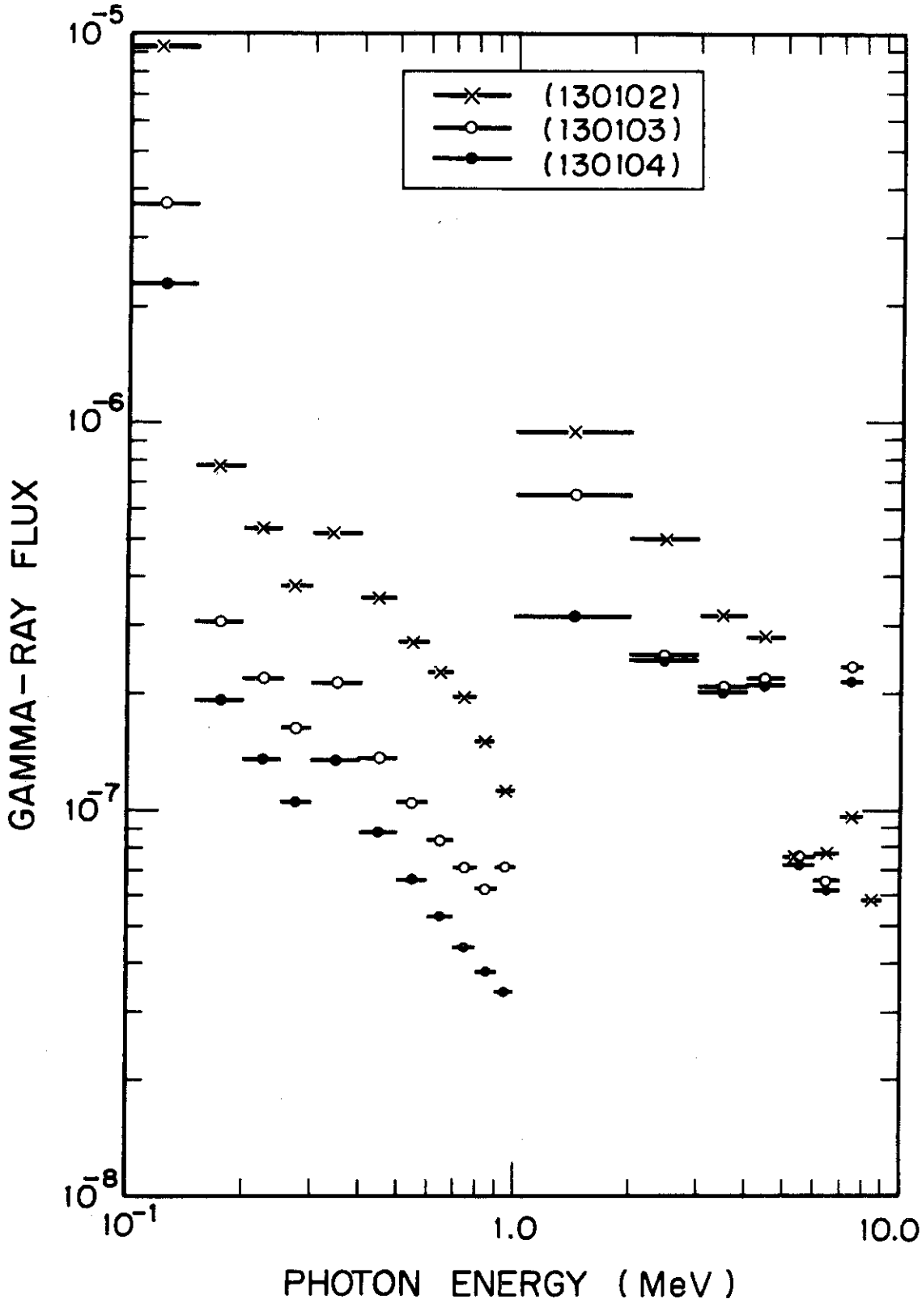

Fig. 4 Gamma-ray flux at 60 cm from the center of aluminum sphere with radius 100 cm.

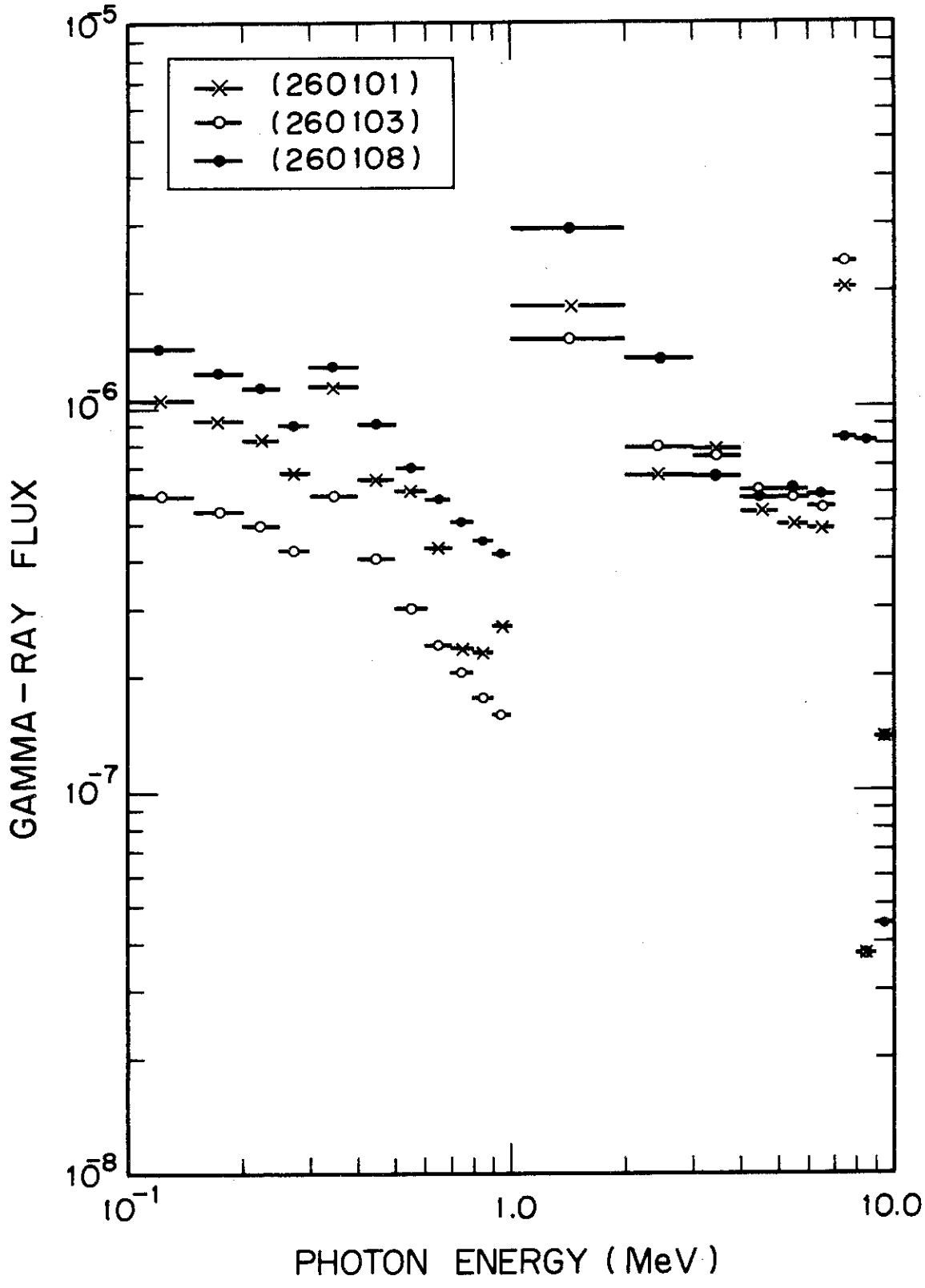

Fig. 5 Gamma-ray flux at 15 cm from the center of iron sphere with radius 25 cm.

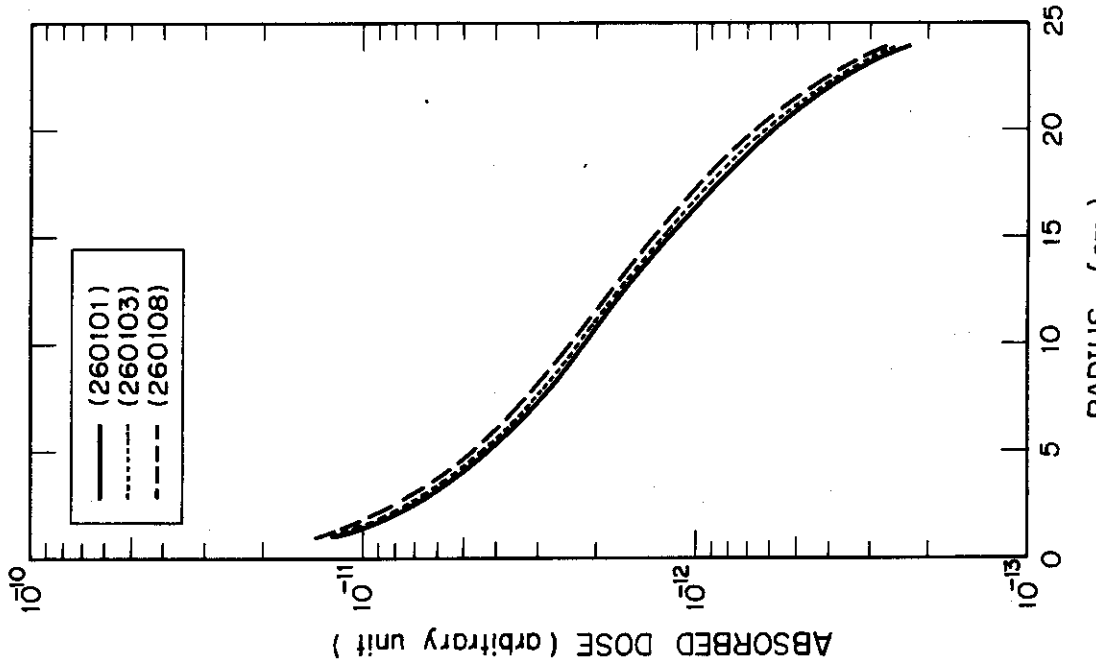

Fig. 7 Absorbed dose distribution in iron sphere.

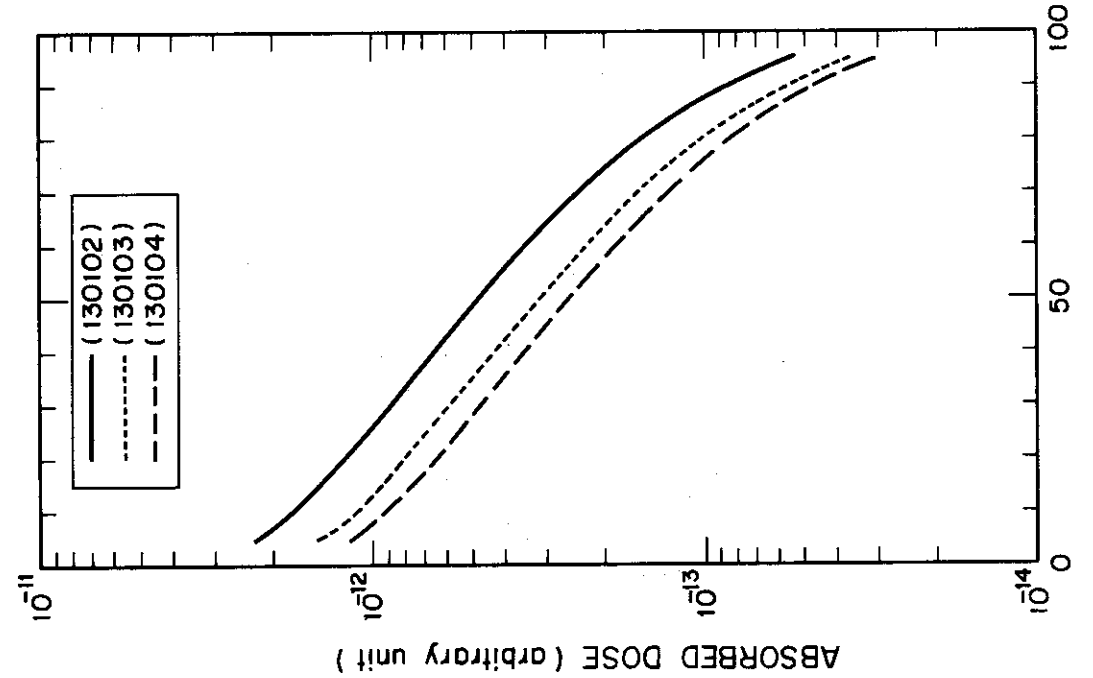

Fig. 6 Absorbed dose distribution in aluminum sphere.

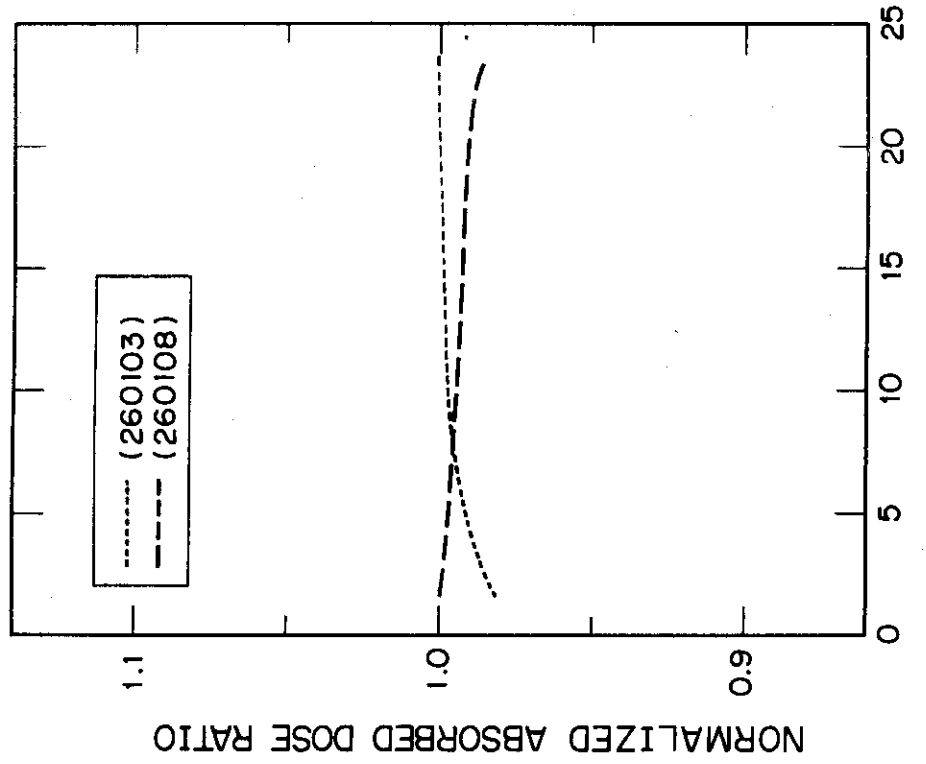

Fig. 9 The ratios of the normalized absorbed doses in the iron sphere by data set 260103 and 260108 to that by data set 260101.

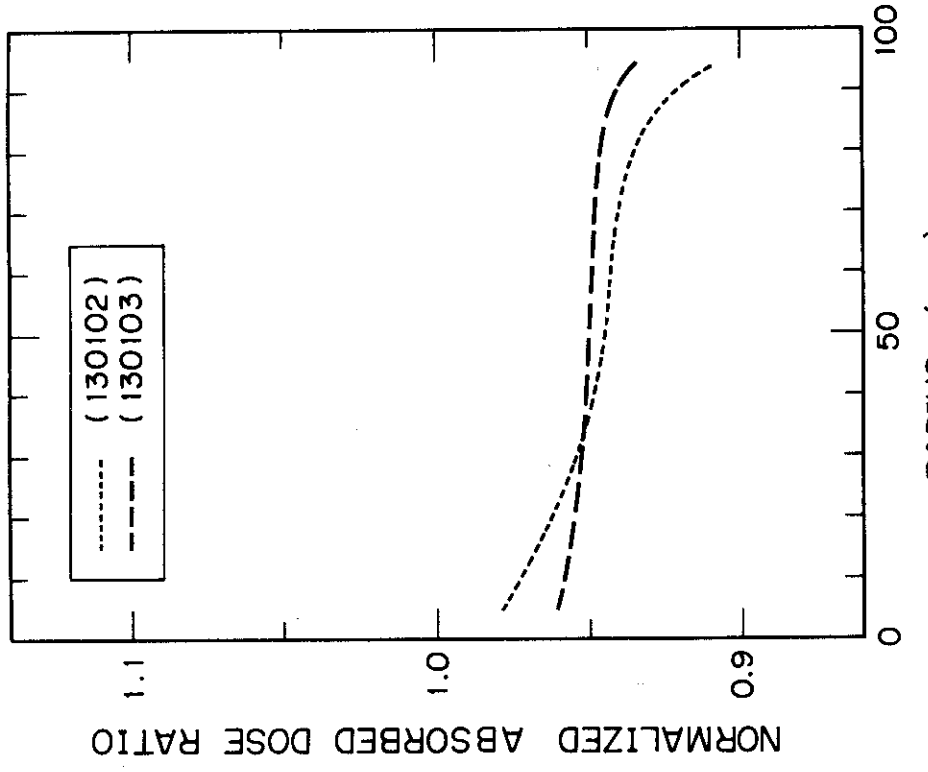

Fig. 8 The ratios of the normalized absorbed doses in the aluminum sphere by data set 130102 and 130103 to that by data set 130104.